PERGAMON International Journal of Non-Linear Mechanics 36 (2001) 1123–1133

INTERNATIONAL JOURNAL OF
NON-LINEAR
MECHANICS

www.elsevier.com/locate/ijnonlinmec

Variable parametric pseudo-rigid-body model for large-deflection beams with end loads

Mohammad H. Dado

Department of Mechanical Engineering, Faculty of Engineering and Technology, University of Jordan, Amman, Jordan

Received 1 January 2000; received in revised form 13 June 2000; accepted 10 July 2000

Abstract

This paper presents a variable parametric pseudo-rigid-body model for large-deflection beams with end loads. The values of the applied load (P) and joint stiffness of pseudo-rigid-body model (k) are expressed in terms of its kinematic parameters: the characteristic length (γ) and the "pseudo-rigid-body angle" (Θ). The expressions cover practical range of applications using a single equation for each variable. The accuracy of the expressions is excellent with correlation coefficients of (0.999) and (0.995). The accuracy of the end deflections generated by these expressions is shown to be much more greater than using the constant values for (γ) and (k). The new model is used for the analysis of two compliant mechanisms with different modes of analysis. The advantages of the new model and how it blends itself very smoothly in the analysis algorithm is illustrated through these examples.

Keywords: Large deflections; Compliant mechanisms; Pseudo-rigid-body

1. Introduction

Large-deflection beams gained great interest in the recent years for their application in compliant mechanisms analysis and design. The motion in compliant mechanisms is partially or completely generated by the flexibility of its links beside the mobility provided by the rigid-body joints [1]. Parametric approximation model for large-deflection beams [2] using pseudo-rigid-body model is a practical approach for implementing such beams in compliant mechanisms. In these models, polynomial curve fitting is used to relate the different model parameters and the end load parameters. These relations are valid for specified ranges and values. Optimum values for these parameters were obtained [3,4] by which the error is minimized. These optimum values are useful for certain ranges of the applied force magnitude and orientation. Large deflection beams with end forces and moments are approximated by pseudo-rigid-body model [5–7]. The model presented for this combined load is based on the psuedo-rigid-body model without the end moment. Optimum values for the model parameters are obtained along with the numerical impirical relations to approximate the end deflections. The psuedo-rigid-body model is used in compliant mechanisms in the analysis and synthesis modes [8]. The loop-closure equations are coupled with the virtual work equations to analyse and synthesize compliant four-bar mechanisms using constant optimum values of the model parameters.

E-mail address: dado@ju.edu.jo (M.H. Dado).

0020-7462/01/$ - see front matter
PII: S0020-7462(00)00076-7

In this paper an improved model is proposed. It is based on the psuedo-rigid-body model presented by [2]. Improvement in the model is gained by finding correlation functions between the applied end load (P) and the rigid-body joint stiffness (k) on the one hand and the model kinematic parameters: characteristic length (γ) and the "pseudo-rigid-body angle" (Θ) on the other. It is proven throughout this paper that the proposed correlations predict very accurate results and provide equations that couples very smoothly with the loop-closure equations for the purpose of analysis. Synthesis applications of the proposed model are to be presented in a following paper.

The governing equations of large deflection in beams with end loads is presented in the following section. The variable parametric model is defined next followed by the derivation procedure of the correlation equations. Finally, the model validation and compliant mechanisms examples are presented along with concluding remarks.

2. Large deflection in beams with end loads

Consider the cantilever beam shown in Fig. 1 with loads P and nP at the free end acting along the positive y-axis and the negative x-axis, respectively. The deflected shape of the beam is shown by the dotted line where a and b are the location of the free end along the x-axis and y-axis, respectively. The values of a and b are given by [2] as

$$\frac{a}{l} = \frac{1}{\alpha\sqrt{2}} \int_0^{\theta_0} \frac{\cos\theta}{\sqrt{\lambda - \sin\theta + n\cos\theta}}\, d\theta \tag{1}$$

$$\frac{b}{l} = \frac{1}{\alpha\sqrt{2}} \int_0^{\theta_0} \frac{\sin\theta}{\sqrt{\lambda - \sin\theta + n\cos\theta}}\, d\theta \tag{2}$$

where

$$\alpha = \frac{1}{\sqrt{2}} \int_0^{\theta_0} \frac{d\theta}{\sqrt{\lambda - \sin\theta + n\cos\theta}} \tag{3}$$

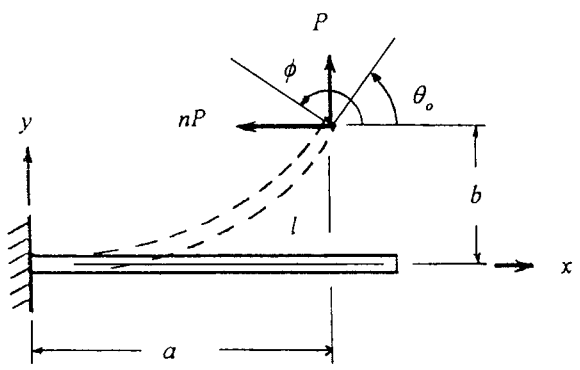

Fig. 1. A flexible cantilever beam subjected to end loads and its deflected geometry.

$$\lambda = \eta\cos(\theta_0 - \phi) \tag{4}$$

$$\eta = \sqrt{1 + n^2} \tag{5}$$

$$\phi = \tan^{-1}\frac{1}{-n} \tag{6}$$

$$\alpha^2 = \frac{Pl^2}{EI}. \tag{7}$$

In Eqs. (1)–(7), θ_0 is the slope angle of the beam axis at the free end, ϕ is the direction of the applied load with respect to the x-axis, E, I, and l are the beam's modulus of elasticity, cross-sectional area moment of inertia and length, respectively. The integrals in Eqs. (1)–(3) are elliptic integrals that could be evaluated numerically. Given the loads P and nP, the free-end location parameters a and b are determined by Eqs. (1) and (2) after evaluating the angle θ_0. However, Eq. (3) relates θ_0 to the load P through α implicitly. Therefore, an iterative procedure is required to find a and b. The iteration process is numerically involved and time consuming. To overcome this difficulty, the solution may start with the given values of θ_0 and ϕ so that α is obtained from Eq. (3). In this way the iteration is avoided but there is no control over the resulting applied load P. However, to make use of the results obtained in this manner a regression procedure is followed in which the parameters of a pseudo-rigid body model of the beam are related to the loads and deflections at the free end of the beam.

3. The pseudo-rigid body model with variable parameters

The pseudo-rigid body model for the flexible beam is shown in Fig. 2 and it is based on the model presented by [2]. However, the new model has parameters that vary with the beams free-end loads and deflections. In Fig. 2, the flexible cantilever beam is represented by a fixed segment with length $l(1-\gamma)$ and a rotating segment with length γl pivoting at the end of the fixed segment. A torsional spring with stiffness k couples the two segments at the pivot. The angle Θ is the "pseudo-rigid-body angle". It defines the angular position of the rotating segment with respect to the fixed segment. The torsional spring is deflected by this angular quantity. The location of the free end of the moving beam segment is to trace the original beam free end when both ends are subjected to the same loads. In contrast to the pseudo-rigid body models presented by [2], the new model finds through regression analysis approximate but quite accurate equations that relate the model parameters as follows:

$$k = f_k(\gamma, \Theta)\frac{EI}{l} \tag{8}$$

and

$$P = f_p(\gamma, \Theta)\frac{EI}{l^2}. \tag{9}$$

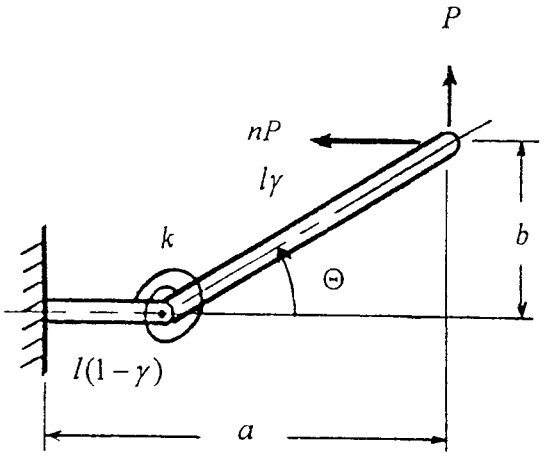

Fig. 2. The pseudo-rigid-body model of the flexible cantilever beam.

Eqs. (8) and (9) express the model's stiffness k and load P in terms of the model's kinematics parameters γ and Θ. The benefit of Eqs. (8) and (9) is realized by considering γ and Θ to be unknown kinematics parameters within the mechanism employing the pseudo-rigid body model. These two additional unknowns are accounted for by the loop closure equations and the static equilibrium equations of the mechanism using the expressions for k and P given by Eqs. (8) and (9). The additional static equations are dependent on the mechanism configuration and loading and on the mode of analysis. In the following section the procedure for obtaining Eqs. (8) and (9) is presented.

4. Regression relations of the pseudo-rigid body model

The regression relations of Eqs. (8) and (9) are obtained through the generation of data sets for γ, Θ, f_k, and f_P covering the range of loads that may be experienced by the beam. The data sets are generated numerically by employing Eqs. (1)–(7). Regression relations are derived so that the values of f_k and f_P are expressed as functions of γ and Θ. The following steps explain this procedure:

Step 1: Discretizing the space of θ_0 and ϕ

A practical range for θ_0 is considered so that $0 < \theta_0 \leqslant \pi$. This range for θ_0 covers most physically realizable cases in compliant mechanism applications. The range $-\pi \leqslant \theta_0 < 0$ is consequently covered by the first range because of symmetry. The discrete values of θ_0 are given by

$$\theta_{0i} = i\Delta\theta_0, \quad i = 1, 2, 3, \ldots, n_t \tag{10}$$

where n_t is the number of points in the space of θ_0. $\Delta\theta_0$ is given by

$$\Delta\theta_0 = \frac{\pi}{n_t}. \tag{11}$$

The range for ϕ is dependent on the corresponding value of θ_0. The value of ϕ must be chosen so that the expression under the radical that appears in Eq. (3) is never negative for the range $0 < \theta \leqslant \theta_0$. It was observed that ϕ must be greater than θ_0 ($\phi \geqslant \theta_0$)

in order to avoid the negative radical. From a physical point of view, it is not possible to have a slope at the free end of the beam that is greater than the slope of the applied force. This establishes the lower limit for ϕ as $\phi_{\min} = \theta_{0i}$. The upper limit is chosen as $\phi_{\max} \prec \pi$. This range for ϕ covers all possible values because of the symmetry of beam deflection and loading. For a given value of θ_{0i}, the discrete values of ϕ are given as

$$\phi_{ij} = \theta_{0i} + (j-1)\Delta\phi_i \quad j = 1, 2, 3, \ldots, m_{ti}, \tag{12}$$

where m_{ti} is the number of points for ϕ at θ_{0i} and $\Delta\phi_i$ is given as

$$\Delta\phi_i = \frac{\pi - \theta_{0i}}{m_{ti}}. \tag{13}$$

The total number of points in the discretized two-dimensional space is

$$N = \sum_{i=0}^{n_t} m_{ti}. \tag{14}$$

Step 2: Evaluating the deflected end positions a and b and the load P

For a given combination of θ_{oi} and ϕ_{ij}, the free-end-deflected position and the vertical load component are evaluated using Eqs. (1)–(3). A numerical integration scheme based on Gaussian quadrature [9] is implemented to evaluate the elliptic integrals present in Eqs. (1)–(3). A 16-point quadrature is chosen in which

$$\int_{x_1}^{x_2} f(x)\,\mathrm{d}x = \frac{x_2 - x_1}{2} \sum_{i=1}^{16} H_i f(t_i), \tag{15}$$

where

$$t_i = x_1 + \frac{x_2 - x_1}{2}(1 + z_i). \tag{16}$$

The values of H_i and z_i are given in Table 1 for $i = 1, \ldots, 8$. For $i = 9, \ldots, 16$, the values of H_i and z_i are obtained through symmetry [9] as $H_{j+8} = H_{9-j}$ and $z_{j+8} = -z_{9-j}$, $(j = 1, \ldots, 8)$.

Step 3: Evaluating the model kinematics parameters γ and Θ and end load P

For given values of a and b found in Step 2, the pseudo-rigid body kinematics parameters are evaluated. From Fig. 2, the kinematics parameters

Table 1
The Gaussian quadrature points (z_i) and weights (H_i) [9]

i	z_i	H_i
1	0.9894009	0.0271525
2	0.9445750	0.0622535
3	0.8656312	0.0951585
4	0.7554044	0.1246290
5	0.6178762	0.1495960
6	0.4580168	0.1691565
7	0.2816036	0.1826034
8	0.0950125	0.1894506

γ and Θ are found as

$$\gamma = \frac{1}{2}\left[1 - \frac{a}{l} + \frac{(b/l)^2}{1 - a/l}\right] \tag{17}$$

and

$$\Theta = \tan^{-1}\left(\frac{b/l}{a/l + \gamma - 1}\right). \tag{18}$$

The free-end load P is computed using the value of α obtained by Step 2 and Eq. (7). The load P is given as

$$P = \frac{EI\alpha^2}{l^2} \tag{19}$$

or

$$P = f_p \frac{EI}{l^2}, \tag{20}$$

where $f_p = \alpha^2$. (21)

At the end of this step, N combinations of (γ, Θ, f_p) exist. Each combination corresponds to a unique loading at the free end.

Step 4. Evaluating the torsional spring stiffness k

The torsional stiffness k for the spring that couples the two segments of the beam is evaluated from the given and computed parameters in the previous steps. From Fig. 2, the internal moment at the pivot is given as

$$M = \left(-\frac{b/l}{\tan\phi} + \left[\frac{a}{l} - (1 - \gamma)\right]\right) Pl. \tag{22}$$

The stiffness k of the spring is therefore given as

$$k = \frac{M}{\Theta} \tag{23}$$

or

$$k = f_k \frac{EI}{l} \tag{24}$$

where

$$f_k = \left(-\frac{b/l}{\tan\phi} + \left[\frac{a}{l} - (1-\gamma) \right] \right) \frac{\alpha^2}{\Theta}. \tag{25}$$

Now, another N combinations consisting of (γ, Θ, f_k) exist. The combinations defined in this step and Step 3 mean that at any given values of γ and Θ, the corresponding values of f_p and f_k exist. Therefore, these combinations form the regression data needed to obtain the relations given in Eqs. (8) and (9).

Step 5: Deriving the regression relations from the generated combinations

The regression functions $f_k(\gamma, \Theta)$ and $f_p(\gamma, \Theta)$ are obtained through regression analysis using the data generated in Steps 3 and 4. A two variable polynomial fit is used to form the regression relation for each function. Deriving the relation for a general case, the two variable polynomial fit is defined as

$$f(x,y) = \sum_{i=1}^{n_x} \sum_{j=1}^{n_y} a_{ij} x^{m_i} y^{l_j}, \tag{26}$$

where $f(x,y)$ is the approximate function, n_x and n_y are the number of terms for the independent variables x and y, respectively. The integers m_i and l_j are the selected powers for x and y and a_{ij} are the polynomial coefficients to be determined by minimizing the error between the approximate function and the actual values of the dependent variable given by the regression data. The sum of the square of the error for the N data points is given by

$$E_T = \sum_{q=1}^{N} (F_q - f(x_q, y_q))^2, \tag{27}$$

where F_q is the actual value of the dependent variable at the qth data point, x_q and y_q are the values of the independent variables at the same point. The error E_T is minimum when

$$\frac{\partial E_T}{\partial a_{ij}} = 0 \quad \text{for } i = 1,2,3,\ldots,n_x$$

and

$$j = 1,2,3,\ldots,n_y. \tag{28}$$

Eqs. (28) produces a set of $K = n_x \times n_y$ simultaneous equations defined as

$$[A_{rs}]_{K\times K}\{b_r\}_{K\times 1} = \{c_r\}_{K\times 1}, \tag{29}$$

where the indices r and s are defined as

$$r(i_r, j_r) = (i_r - 1)n_y + j_r,$$

$$(i_r = 1,2,3,\ldots,n_x,\ j_r = 1,2,3,\ldots,n_y), \tag{30}$$

$$s(i_s, j_s) = (i_s - 1)n_y + j_s,$$

$$(i_s = 1,2,3,\ldots,n_x,\ j_s = 1,2,3,\ldots,n_y) \tag{31}$$

with this definition for the indices r and s, the terms in Eq. (29) are defined as

$$A_{r(i_r,j_r),s(i_s,j_s)} = \sum_{q=1}^{N} x_q^{m_{i_r}} y_q^{l_{j_r}} x_q^{m_{i_s}} y_q^{l_{j_s}}, \tag{32}$$

$$b_{r(i_r,j_r)} = a_{i_r,j_r} \tag{33}$$

and

$$c_{r(i_r,j_r)} = \sum_{q=1}^{N} F_q x_q^{m_{i_r}} y_q^{l_{j_r}}. \tag{34}$$

Solving the linear system of equations in (29) leads to the determination of the regression polynomial coefficients a_{ij}.

4.1. Regression analysis results

The regression analysis procedure is applied for $n_t = 25$ and $m_{tj} = n_t - j$, $(j = 1,2,3,\ldots,n_t)$ so that $\Delta\phi_i = \Delta\theta_0$ for any i (see Eqs. (10)–(13)). This choice for n produces 300 data sets $(N = 300)$ for $(\gamma, \Theta, f_k, f_P)$. The regression coefficients corresponding to the selected powers of γ and Θ for the functions $f_k(\gamma, \Theta)$ and $f_P(\gamma, \Theta)$ are listed in Tables 2 and 3. The correlation coefficient (r^2) as defined by [2], equals 0.99906 for $f_k(\gamma, \Theta)$ and 0.99507 for $f_P(\gamma, \Theta)$.

Table 2
The regression coefficients (a_{ij}^k) corresponding to the selected powers (m_i^k) and (l_j^k) of γ and Θ for $f_k(\gamma,\Theta)$

l_j^k	$m_i^k=0$	$m_i^k=1$	$m_i^k=2$	$m_i^k=3$
0	38.887320	−46.116660	−57.806580	72.044230
2	20.552660	−48.042440	28.604680	−0.5203912
4	−2.976025	4.058771	2.128592	−3.227307
6	−0.1614047	0.6910204	−0.8980537	0.3618954

Table 3
The regression coefficients (a_{ij}^P) corresponding to the selected powers (m_i^P) and (l_j^P) of γ and Θ for $f_P(\gamma,\Theta)$

l_j^P	$m_i^P=0$	$m_i^P=1$	$m_i^P=2$	$m_i^P=3$
1	668.957300	−1059.420000	−588.385000	1081.292000
3	319.577300	−726.299000	437.309200	−32.938720
5	−24.293850	19.232190	52.777420	−48.507020
7	−5.712759	13.005080	−7.152013	−0.3379520

The regression functions are defined as

$$f_k(\gamma,\Theta)=\sum_{i=1}^{4}\sum_{j=1}^{4}a_{ij}^k\gamma^{m_i^k}\Theta^{l_j^k}, \tag{35}$$

$$f_P(\gamma,\Theta)=\sum_{i=1}^{4}\sum_{j=1}^{4}a_{ij}^P\gamma^{m_i^P}\Theta^{l_j^P}. \tag{36}$$

As seen in Table 2 the powers of Θ are even for $f_k(\gamma,\Theta)$. This choice is made in order to have symmetrical positive values for $f_k(\gamma,\Theta)$ for positive and negative values of Θ. In Table 3, the powers of Θ are odd in order for $f_P(\gamma,\Theta)$ to have equal magnitudes but opposite signs as Θ changes signs. These requirements are necessary to take advantage of the symmetry of the beam deflection in relation with the applied end load for positive and negative values of Θ.

4.2. Regression functions validation and comparison with published data

The regression functions derived in the previous section are validated by solving Eqs. (1)–(3) for the free-end deflections iteratively. For the given values of α and n, Eq. (3) is solved iterativitly for θ_0. Using the value of θ_0 and

$$G_1(\gamma,\Theta)=\alpha^2-f_P(\gamma,\Theta)=0, \tag{37}$$

$$G_2(\gamma,\Theta)=K-f_k(\gamma,\Theta)=0, \tag{38}$$

$$\text{where } K=\frac{\gamma\alpha^2}{\Theta}(\cos\Theta+n\sin\Theta), \tag{39}$$

the free-end deflections are determined as

$$\frac{a}{l}=(1-\gamma)+\gamma\cos\Theta \tag{40}$$

and

$$\frac{b}{l}=\gamma\sin\Theta. \tag{41}$$

Figs. 3 and 4 show plots of the deflection ratios against the end load for several representative values of the load application angle ϕ. These plots are for the reference values using the elliptic integrals and for the regression function model. The agreement between the two results is excellent as could be seen from the figures. For the purpose of comparison, end deflections are evaluated using the approximate values of $\gamma=0.85$ and $K=2.65$ given

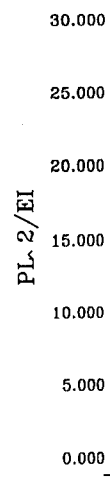

Fig. 3. The
different lo
regression

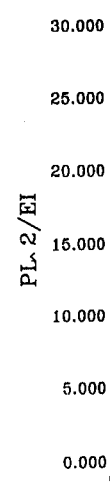

Fig. 4. Th
different lo
regression

by [4]. I
Eq. (39)
puted by
results in

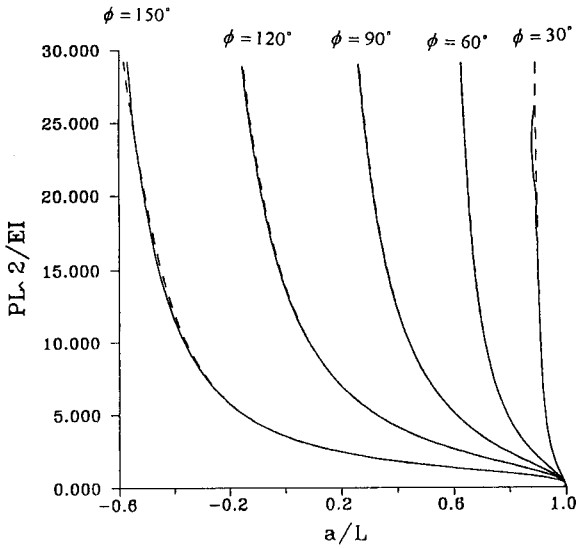

Fig. 3. The axial deflection ratio vs. the end-load ratio for different load application angles: (—) elliptic integrals; (- - - -) regression functions.

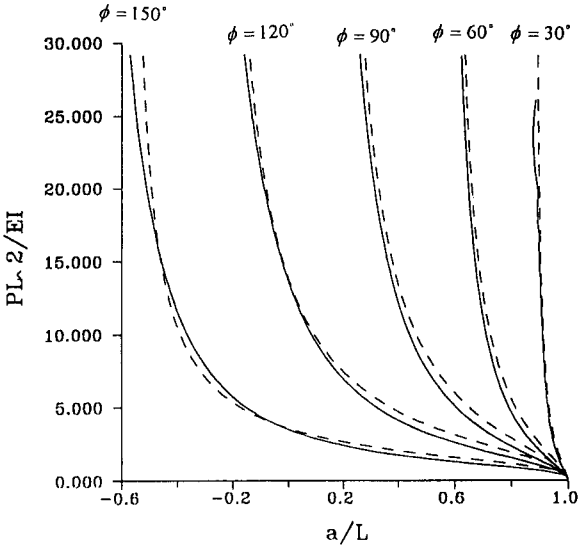

Fig. 5. The axial deflection ratio vs. the end-load ratio for different load application angles: (—) elliptic integrals; (- - - -) constant model parameters.

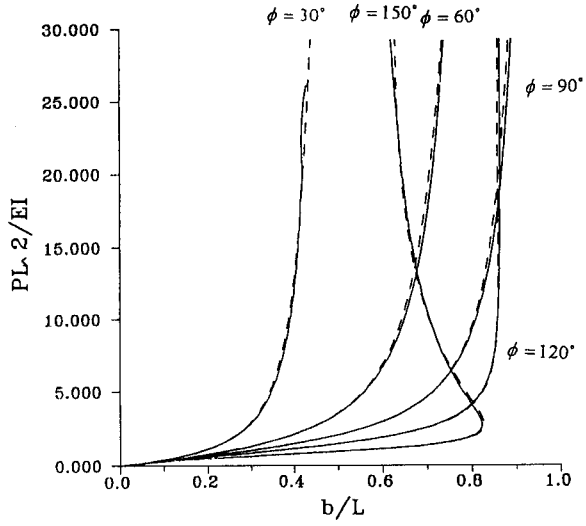

Fig. 4. The normal deflection ratio vs. the end-load ratio for different load application angles: (—) elliptic integrals; (- - - -) regression functions.

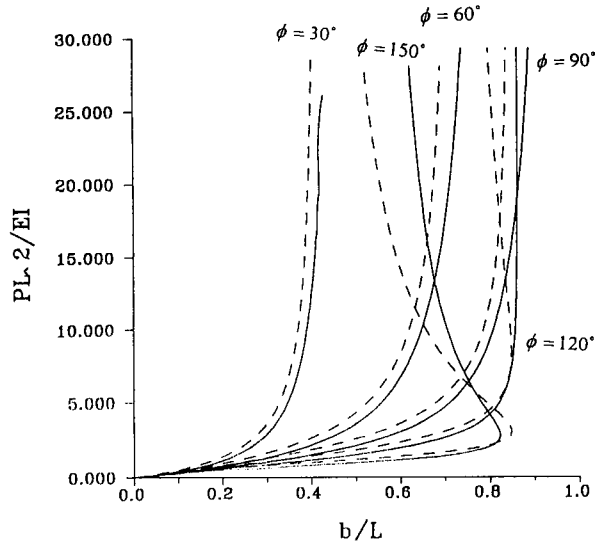

Fig. 6. The normal deflection ratio vs. the end-load ratio for different load application angles: (—) elliptic integrals; (- - - -) constant model parameters.

by [4]. In this case Θ is evaluated iteretively using Eq. (39) and the free-end deflection ratios are computed by Eqs. (40) and (41). Figs. 5 and 6 show the results in comparison with the reference values obtained by evaluating the elliptic integrals. It is quite obvious that non-negligible errors exist in using these approximate values. However, these approximations are useful for obtaining initial guesses for

the variables when solving the non-linear equations resulting from the regression functions.

5. Examples

Two compliant mechanisms are considered for analysis to demonstrate the advantages of the new model. The first mechanism is the compliant slider-crank mechanisms considered by [2]. The mechanism is analyzed again using the development presented in this paper for comparison purposes. As the second example, the same mechanism is analyzed after introducing coulomb dry friction along the slider path. The second compliant mechanism is a four-bar mechanism driven with known torque at the input link.

5.1. The slider-crank mechanism

Figs. 7(a) and (b) show the compliant slider crank mechanism and its pseudo-rigid-body model, respectively. This mechanism has a flexible coupler with length l equals 5.0 units, a crank with length r equals 3.0 units and an offset e equals 0.5 units. The mechanism is driven by the crank with a torque T. The flexible coupler is fixed to the slider block so that it is parallel to the slider path when not assembled. It is required to plot the slider position x_B and the driving torque T against the crank angle φ. The loop closure equations for the mechanism are

$$x_B - r\cos\varphi - l(1-\gamma) - l\gamma\cos\Theta = 0, \tag{42}$$

$$r\sin\varphi - l\gamma\sin\Theta - e = 0. \tag{43}$$

The static moment equilibrium equation at the joint of the pseudo-rigid-body model of the flexible coupler link is given as

$$F_x l\gamma\sin\Theta + f_P(\gamma,\Theta)\frac{EI}{l^2}l\gamma\cos\Theta - f_k(\gamma,\Theta)\frac{EI}{l}\Theta = 0, \tag{44}$$

where EI is the flexural stiffness of the link, F_x is the force acting on the slider parallel to its path. For the first example, $F_x = 0$. However, for the case in

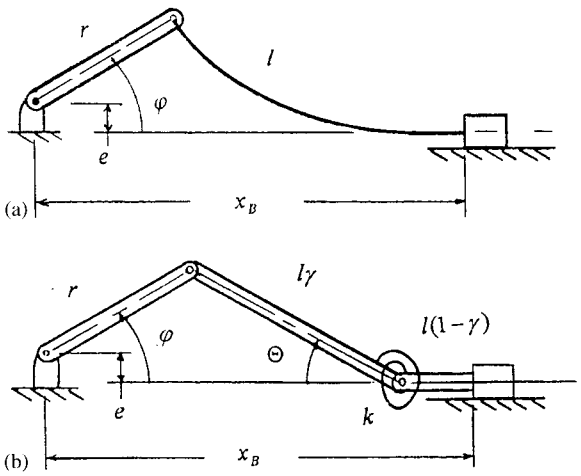

Fig. 7. (a) The compliant slider-crank mechanism; (b) The pseudo-rigid-body model of the mechanism.

which dry friction exists along the slider path, F_x is given by

$$F_x = \operatorname{sgn}\mu f_p(\gamma,\Theta)\frac{EI}{l^2}, \tag{45}$$

where μ is the dry friction coefficient and (sgn) is either $(+1)$ or (-1) depending on the direction of motion of the slider. The value of μ is set to 0.3. The value of (sgn) is defined using the virtual displacement relation between φ and x_B obtained by taking the differentials of Eqs. (42) and (43) as

$$\delta x_B = -\left(r\sin\varphi + \frac{r\cos\varphi\sin\Theta}{\cos\Theta}\right)\delta\varphi. \tag{46}$$

Using Eq. (46), (sgn) is given by

$$\operatorname{sgn} = -\frac{\left(r\sin\varphi + \dfrac{r\cos\varphi\sin\Theta}{\cos\Theta}\right)}{\left|r\sin\varphi + \dfrac{r\cos\varphi\sin\Theta}{\cos\Theta}\right|}. \tag{47}$$

The unknowns in Eqs. (42)–(44) are γ, Θ and x_B. Newton–Raphson method with numerical differentiation is used to solve the set of three non-linear algebraic equations. Fig. 8 plots the slider position (x_B) against the crank angle (φ) for both cases. No significant difference exists between the two cases

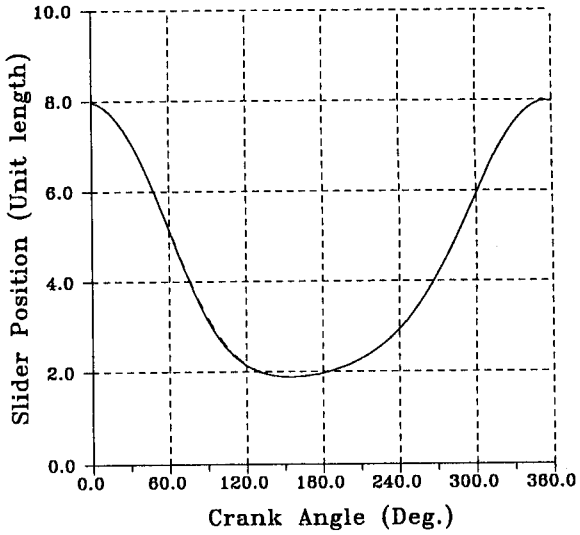

Fig. 8. The slider position vs. the crank angle for the compliant slider-crank mechanism: (—) without friction; (- - - -) with friction.

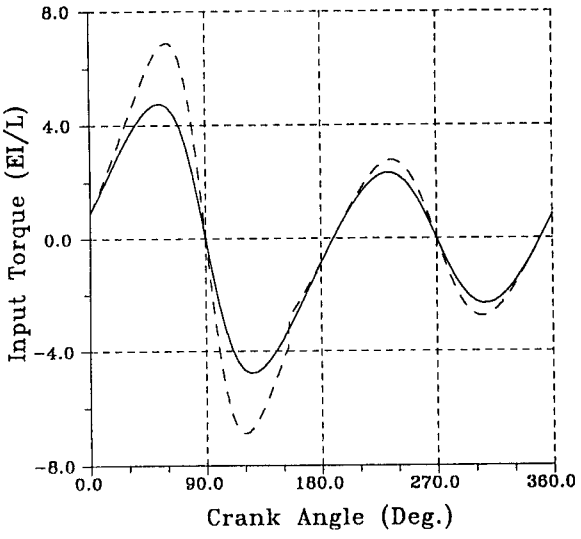

Fig. 9. The driving torque at the crank vs. the crank angle for the compliant slider-crank mechanism: (—) without friction; (- - - -) with friction.

for the slider position. The driving torque is determined by writing the moment equilibrium equation for the crank as

$$T = -F_x r \sin\varphi + f_P(\gamma, \Theta)\frac{EI}{l^2} r \cos\varphi. \tag{48}$$

The magnitude of the torque for the case with friction is larger as can be expected. From Fig. 9, the discontinuity in the torque is noticed at the region within which the slider changes direction. The results for the slider position for the case without friction match exactly with those given in [2]. However, the results for the driving torque does not match in magnitude but compare well with the trend. It is very hard to explain this disagreement in the view of the exact match for the slider position. Fig. 10 shows the plots of the normal and horizontal force applied on the flexible coupler link of the mechanism for the two cases. The magnitude of the normal force is significantly increased due to friction in the first half-cycle but as seen in the figure the frictional horizontal force is negative. Therefore, the moments produced by horizontal and normal force are opposite in directions during this half-cycle. In the second half-cycle the change in the

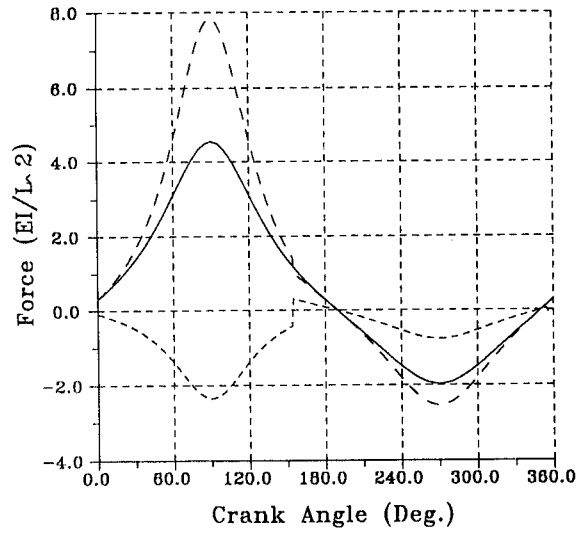

Fig. 10. Compliant link forces for the compliant slider-crank mechanism. (Normal force: (—) without friction; (- - - -) with friction. Frictional force: - - - -).

magnitude of the normal force is very moderate. This analysis of Fig. 10 explains the very little difference between the two cases in the slider path vs. the crank angle.

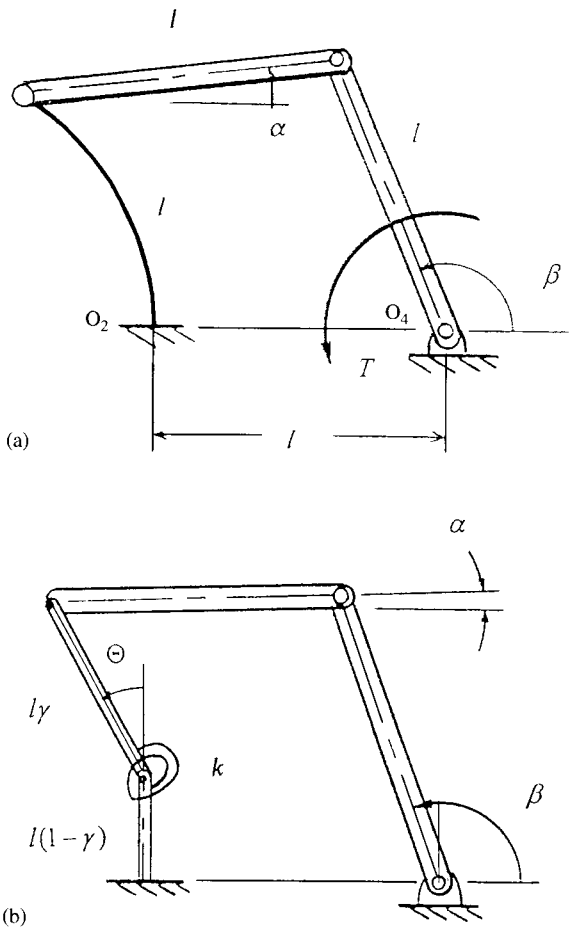

Fig. 11. (a) The compliant four-bar mechanism; (b) the pseudo-rigid-body model of the mechanism.

5.2. The four-bar mechanism

The second example is a four-bar mechanism with equal link lengths having l units length each as shown in Fig. 11(a). The link at O_2 is flexible and fixed to the ground in the vertical position. Fig. 11(b) shows the equivalent pseudo-rigid-body model. The mechanism is driven by known torque (T) at O_4. It is required to plot the link angles β,α and Θ against the driving torque (T). The loop closure equations and the static equilibrium equations are given as

$$\cos\alpha - \cos\beta - \gamma\sin\Theta - 1 = 0, \tag{49}$$

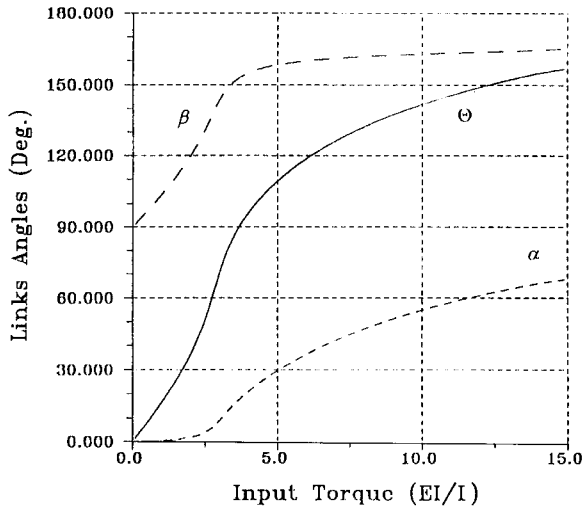

Fig. 12. Links angles vs. driving torque for the compliant four-bar mechanism.

$$1 - \gamma + \gamma\cos\Theta + \sin\alpha - \sin\beta = 0, \tag{50}$$

$$f_P(\gamma,\Theta)\frac{EI}{l^2} - F_c\cos\alpha = 0, \tag{51}$$

$$f_k(\gamma,\Theta)\frac{EI}{l}\Theta - F_c\cos(\Theta-\alpha)l\gamma = 0, \tag{52}$$

where F_c is the axial force in the coupler link and it is given in terms of the driving torque as

$$F_c = \frac{T}{\sin(\beta-\alpha)l}. \tag{53}$$

The unknowns in this model are γ, Θ, α, and β. They are solved by using Eqs. (49)–(53). Fig. 12 plots the values for the three angles Θ, α, and β against the input torque (T). Fig. 13 plots the values of the characteristic radius γ and Fig. 14 plots the values of the equivalent spring k of the pseudo-rigid-body model. The change in γ is limited and has an average value of 0.85. However, the value of k varies in a wide range between 2.0 and 4.5. In this

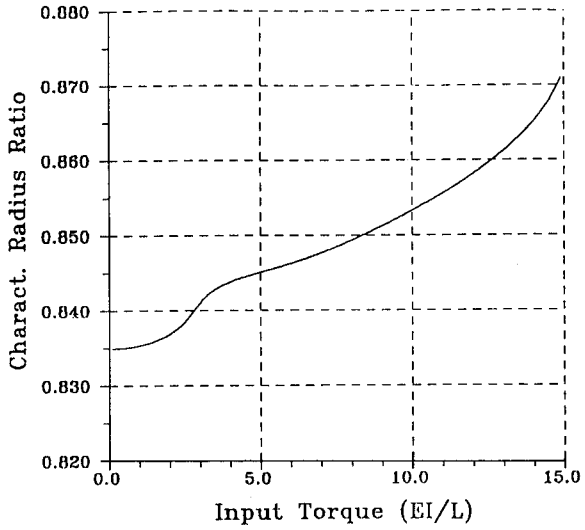

Fig. 13. Characteristic radius ratio of the pseudo-rigid-body model of the compliant link vs. the input torque for the compliant four-bar mechanism.

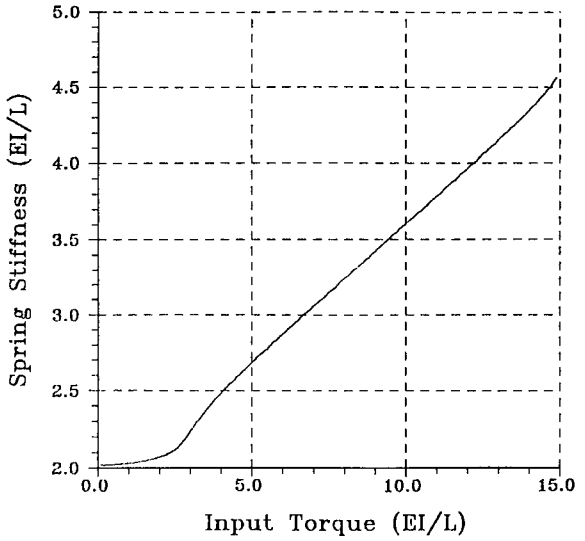

Fig. 14. Joint stiffness of the pseudo-rigid-body model of the compliant link vs. the input torque for the compliant four-bar mechanism.

example the value of Θ exceeded 150° taking the model to its limits without losing the stability of the solution.

6. Conclusions

This paper presented a new pseudo-rigid-body model for large-deflection beams with end loads. Correlation equations relate the model kinematics parameters and the applied loads with high accuracy. These relations cover a wide and practical range of end loads without segmenting the model parameters into zones or regions for the validity of equations. In addition, the correlation equations are formulated in a manner that simplifies the modeling of compliant mechanisms since they couple very smoothly with the mechanisms loop-closure equations. The model is verified by comparing its results with the iterative solution of the elliptic integral equations in that model. Through this analysis the advantages of the model were illustrated.

References

[1] H. Nahvi, Static and dynamic analysis of compliant mechanisms containing highly flexible members, Ph.D. Dissertation, Purdue University, 1991.

[2] L. Howell, A. Midha, Parametric deflection approximations for end-loaded, large-deflection beams in compliant mechanisms, ASME J. Mech. Des. 117 (1) (1995) 156–165.

[3] L. Howell, A. Midha, T.W. Norton, Evaluation of equivalent spring stiffness for use in a pseudo-rigid-body model of large-deflection compliant mechanisms, ASME J. Mech. Des. 118 (1) (1996) 125–131.

[4] L. Howell, Compliant mechanisms class notes, Mechanical Engineering Department, Brigham Young University, Provo, Utah, 1999.

[5] L. Howell, The design and analysis of large-deflection members in compliant mechanisms, M.S. Thesis, Purdue University, West Lafayette, Indiana, 1991.

[6] A. Saxena, A new pseudo-rigid-body model for flexible members in compliant mechanisms, Masters Thesis, University of Toledo, Toledo, Ohio, 1997.

[7] A. Saxena, S.N. Kramer, A simple and accurate method for determining large deflections in compliant mechanisms subjected to end forces and moments, ASME J. Mech. Des. 120 (3) (1998) 392–400.

[8] L. Howell, A. Midha, A loop-closure theory for the analysis and synthesis of compliant mechanisms, ASME J. Mech. Des. 118 (1) (1996) 121–125.

[9] W.L. Beyer (Ed.), Standard Mathematical Tables, CRC Press, Inc., Boca Raton, FL, 1987.